RAMAN AND X-RAY ABSORPTION SPECTROSCOPY INVESTIGATIONS OF THE STRUCTURE AND Ru-Mn VALENCE STATES OF $Li_2Mn_{0.9}Ru_{0.1}O_3$**

B. Singh [1*], P. Singh [1], M. Gupta [2]

[1] Materials Chemistry Lab, Centre of Material Sciences at University of Allahabad, Prayagraj-211002, India; e-mail: braj.iit@gmail.com, brajendr@allduniv.ac.in
[2] UGC DAE Consortium for Scientific Research, University Campus, Indore-452017, India

We report the effect of the sintering temperature on the structure and valence states of Ru-Mn in $Li_2Mn_{0.9}Ru_{0.1}O_3$. These effects are explored by synchrotron X-ray diffraction patterns, Raman and X-ray absorption spectroscopy spectra (analysis of the Ru-M_4, Mn-$L_{2,3}$, and O-K edges). Ru doping at the Mn site in Li_2MnO_3 changes the lattice parameters of the parent Li_2MnO_3. $Li_2Mn_{0.9}Ru_{0.1}O_3$ sintered at 950°C shows two peaks of the Ru-M_4 absorption edge. These peaks confirm the presence of mixed valence states Ru^{+4} and Ru^{+5}. The compound $Li_2Mn_{0.9}Ru_{0.1}O_3$ sintered at 1050°C shows only one peak of the Ru-M_4 absorption edge, which reveals the presence of the Ru^{+4} valence state. The Mn-L_3 absorption edge of $Li_2Mn_{0.9}Ru_{0.1}O_3$ shifts towards lower energy in comparison to the absorption edge of Li_2MnO_3. The O-K absorption edge of $Li_2Mn_{0.9}Ru_{0.1}O_3$ shows the origin of a new peak in comparison to the absorption edge of Li_2MnO_3 due to the presence of Mn^{+3} – O hybridization in $Li_2Mn_{0.9}Ru_{0.1}O_3$ sintered at 950°C. The Raman spectrum of $Li_2Mn_{0.9}Ru_{0.1}O_3$ shows splitting and peak shifting with the change in the sintering conditions. The presence of mixed valences Mn^{+3}, Mn^{+4}, Ru^{+4}, and Ru^{+5} in the lattice of $Li_2Mn_{0.9}Ru_{0.1}O_3$ sintered at 950°C may affect the charge–discharge properties of the $Li_2Mn_{0.9}Ru_{0.1}O_3$ cathode.

Keywords: *synchrotron X-ray, Raman spectroscopy, mixed valence, M_4 absorption edge, O-K absorption edge.*

ИССЛЕДОВАНИЕ СТРУКТУРЫ И ВАЛЕНТНЫХ СОСТОЯНИЙ Ru-Mn В $Li_2Mn_{0.9}Ru_{0.1}O_3$ МЕТОДАМИ КОМБИНАЦИОННОГО РАССЕЯНИЯ СВЕТА И РЕНТГЕНОВСКОЙ СПЕКТРОСКОПИИ ПОГЛОЩЕНИЯ

B. Singh [1*], P. Singh [1], M. Gupta [2]

УДК 535.375.5

[1] Центр материаловедения Университета Аллахабада, Праяградж-211002, Индия; e-mail: braj.iit@gmail.com, brajendr@allduniv.ac.in
[2] Консорциум UGC DAE по научным исследованиям, Университетский городок, Индор-452017, Индия

(Поступила 1 июля 2020)

Проанализировано влияние температуры спекания на структуру и валентные состояния Ru-Mn в $Li_2Mn_{0.9}Ru_{0.1}O_3$. Эффекты исследованы с помощью синхротронных рентгенограмм, спектров комбинационного рассеяния и спектров рентгеновской спектроскопии поглощения (анализ края поглощения Ru-M_4, Mn-$L_{2,3}$ и O-K). Допирование Ru в узле Mn в Li_2MnO_3 изменяет параметры решетки исходного вещества Li_2MnO_3. В спектре $Li_2Mn_{0.9}Ru_{0.1}O_3$, спеченного при 950°C, два максимума края поглощения Ru-M_4 подтверждают наличие смешанных валентных состояний Ru^{+4} и Ru^{+5}. Соединение $Li_2Mn_{0.9}Ru_{0.1}O_3$, спеченное при 1050°C, показывает только один максимум Ru-M_4, что подтверждает наличие валентного состояния Ru^{+4}. Край поглощения Mn-L_3 для $Li_2Mn_{0.9}Ru_{0.1}O_3$ смещается

** Full text is published in JAS V. 88, No. 4 (http://springer.com/journal/10812) and in electronic version of ZhPS V. 88, No. 4 (http://www.elibrary.ru/title_about.asp?id=7318; sales@elibrary.ru).

в сторону более низкой энергии по сравнению с Li_2MnO_3. Из-за наличия гибридизации Mn^{+3}-O в спеченном при 950°C веществе $Li_2Mn_{0.9}Ru_{0.1}O_3$ край поглощения O-K $Li_2Mn_{0.9}Ru_{0.1}O_3$ обнаруживает новый максимум по сравнению с Li_2MnO_3. Спектр комбинационного рассеяния $Li_2Mn_{0.9}Ru_{0.1}O_3$ показывает расщепление и сдвиг пика при изменении условий спекания. Наличие смешанных валентностей Mn^{+3}, Mn^{+4}, Ru^{+4} и Ru^{+5} в решетке спеченного при температуре 950°C $Li_2Mn_{0.9}Ru_{0.1}O_3$ может влиять на зарядно-разрядные свойства катода $Li_2Mn_{0.9}Ru_{0.1}O_3$.

Ключевые слова: *синхротронные рентгеновские лучи, спектроскопия комбинационного рассеяния, смешанная валентность, край поглощения M_4, край поглощения O-K.*

Introduction. Lithium manganese oxides are used as positive electrodes for rechargeable lithium batteries due to their low cost, low toxicity, and superior safety [1–3]. Spinel $LiMn_2O_4$, Co, and Ni substituted $LiMnO_2$ are prone to show Li intercalation due to the presence of mixed valences Mn^{+3} and Mn^{+4} [1–3]. The structure of Li_2MnO_3 is similar to the $LiCoO_2$ and $LiNiO_2$structures. In Li_2MnO_3, all the octahedral sites are fully occupied and Li intercalation is not possible as long as the Mn element remains in the Mn^{+4} valence state [4]. In perovskite structures, Ru^{+4} doping at Mn^{+4} causes redox interactions between these valence states, and Ru^{+4} partially changes to Ru^{+5} along with the reduction of Mn^{+4} to the Mn^{+3} valence state [5]. Lyu et al. showed the presence of the Ru^{+4} valence state with the presence of Mn^{+4} in Ru doped Li_2MnO_3 synthesized at 950°C [6]. Sathiya et al. showed the presence of the Ru^{+5} valence state in $Li_2Ru_{0.75}Sn_{0.25}O_3$ [7]. Mori et al. prepared $Li_2Mn_{0.6}Ru_{0.4}O_3$ at 1200°C and showed the involvement of the Ru^{+4}/Ru^{+5} redox pair during the charge and discharge process in $Li_2Mn_{0.6}Ru_{0.4}O_3$ [8]. Sathiya et al. showed the Mn^{+4} and Ru^{+4} valence states in $Li_2Mn_{0.5}Ru_{0.5}O_3$ prepared at 950°C [4]. Various groups of researchers have reported the presence of the Ru^{+4} valence state in Ru doped Li_2MnO_3, which is further converted into the Ru^{+4} and Ru^{+5} valence states during the cycle of charge/discharge [4, 6, 8]. The presence of a single valence state Ru^{+4} in the sintered compound and its conversion into the Ru^{+4} and Ru^{+5} valence states of Ru are in contrast with the results reported on the Ru doped perovskite and spinel compounds [9–11]. Singh et al. showed the presence of mixed valences of Mn^{+3}/Mn^{+4} and Ru^{+4}/Ru^{+5} in the $L_{2,3}$ absorption edge of sintered $La_{0.7}Ca_{0.3}Mn_{1-x}Ru_xO_3$ [9, 10]. Reddy et al. showed the Mn^{+3}/Mn^{+4} and Ru^{+4}/Ru^{+5} valence states in spinel-structured sintered $LiMn_{2-x}Ru_xO_4$ compositions [11]. Zhou et al. showed the presence of the Ru^{+4} valence state in RuO_2 using $M_{4,5}$ edge absorption spectra [12]. Harano et al. showed the presence of the Ru^{+4} valence state in $La_{0.6}Sr_{0.4}Mn_{0.95}Ru_{0.05}O_3$ using $M_{2,3}$ edge absorption spectra [13]. In our recently published research paper, we showed the presence of mixed valence states of Ru-Mn in $Li_2Mn_{0.9}Ru_{0.1}O_3$ [14]. In this paper, we have documented the role of sintering conditions in bringing about the mixed valences of Ru and their effect on the structure of the $Li_2Mn_{0.9}Ru_{0.1}O_3$ composition.

Experimental. Polycrystalline $Li_2Mn_{1-x}Ru_xO_3$ (x = 0, 0.1) samples were prepared by the high- temperature solid state reaction route. In the preparation process, we weighed the stoichiometric amount of high purity $LiOH.H_2O$, MnO_2, and RuO_2. The samples were calcined at 950°C for 12 h and sintered at 950/1050°C for 12 h by keeping the heating rate at 5°C/min in an ambient atmosphere. The $Sr_4Ru_2O_9$ sample was prepared by taking the stoichiometric amount of high purity $SrCO_3$ and RuO_2. The precursors were calcined at 850°C for 36 h in an oxygen atmosphere and subsequently sintered at 950°C for 36 h in a tubular furnace. $LaMnO_3$ and $LaMn_{0.8}Ru_{0.2}O_3$ samples were prepared by taking the stoichiometric amount of high purity La_2O_3, MnO_2, and RuO_2 oxides. The precursors were calcined at 900°C for 24 h and sintered at 1050°C for 24 h. The X-ray powder diffraction patterns using synchrotron radiation (λ = 1.09 Å) were recorded in the angle range from 10 to 70 degrees at room temperature at the Indian beamline BL-18B, Photon Factory (PF), KEK, Tsukuba, Japan. A Renishaw micro-Raman spectrometer (model RM-2000) and a focused Ar^+ laser beam of 514-nm using a Leica microscope were used to record Raman spectra. The incident laser power was attenuated to 2 mW, and the data acquisition time was set to 50 s to record the data for all the samples. The Raman spectra were recorded using a Peltier air-cooled CCD detector in the range 100–3200 cm^{-1} with a spectral resolution of ~2cm^{-1}. X-ray absorption spectroscopy (XAS) measurements for the Mn $L_{2,3}$, and Ru M_4 edges were performed at the Soft X-ray absorption spectroscopy (SXAS) beamline (BL-01) of the INDUS 2 synchrotron source (2.5 GeV, 300 mA) at the Raja Ramanna Centre for Advanced Technology (RRCAT), Indore, India. SXAS data were collected in the total electron yield (TEY) mode.

Results and discussion. We synthesized the Li_2MnO_3 and $Li_2Mn_{0.9}Ru_{0.1}O_3$ compositions by sintering at 950 and 1050°C. We recorded the synchrotron X-ray powder diffraction patterns for all the four compositions, and they show the single phase. Figure 1 shows the X-ray diffraction (XRD) patterns of $Li_2Mn_{0.9}Ru_{0.1}O_3$ synthesized at 950 and 1050°C.

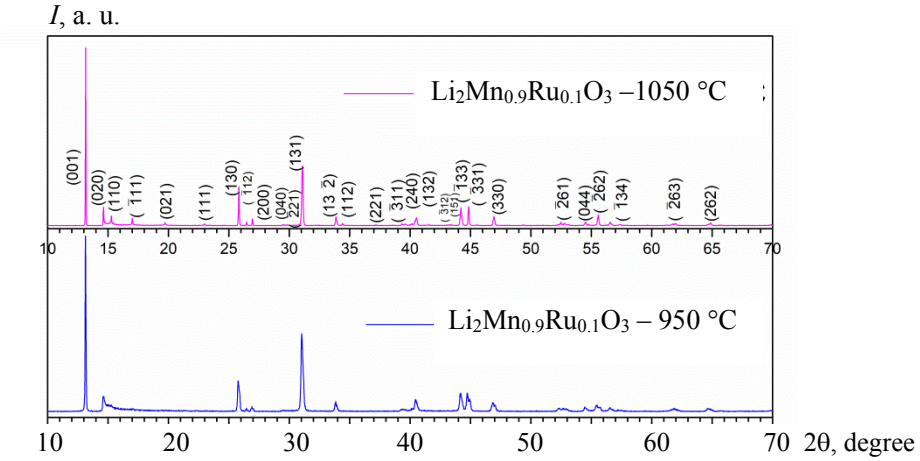

Fig. 1. Synchrotron X-ray diffraction patterns of the Ru-doped Li_2MnO_3 compositions

Figure 2 shows the position of (001), (020), (110), (130), (200), and (131) major peaks. We found the position of all the peaks for the initial composition of Li_2MnO_3 sintered at 950 or 1050°C at nearly the same 2θ values. The Ru doped compositions show the change in the position of peaks (001), (130), (200), and (131) in comparison to the XRD patterns of the initial composition. Shifting the peaks shows the change in the lattice due to the Ru doping at the Mn site in Li_2MnO_3. When we compare the XRD patterns for the 950 and 1050°C sintered $Li_2Mn_{0.9}Ru_{0.1}O_3$ samples, we see that the positions of peaks (001), (130), and (131) are not in the same position. These findings show that the change in the lattice parameters occurs when the sintering temperature changes from 950 to 1050°C for $Li_2Mn_{0.9}Ru_{0.1}O_3$. The lattice parameters are shown in Table 1 for all the four compositions, which were calculated by profile fitting in the synchrotron X-ray powder diffraction pat

TABLE 1. Synchrotron X-ray Diffraction Data Acquisition Conditions and Lattice Parameters of $Li_2Mn_{1-x}Ru_xO_3$ (x = 0 and 0.1)

Sintering temperature	Li_2MnO_3		$Li_2Mn_{0.9}Ru_{0.1}O_3$	
	950°C	1050°C	950°C	1050°C
Space group	C2/m	C2/m	C2/m	C2/m
a, Å	4.938	4.938	4.946	4.951
b, Å	8.542	8.541	8.592	8.569
c, Å	5.032	5.037	5.048	5.044
β, deg	109.34	109.38	109.43	109.29
Volume	200.32	200.44	202.49	202.02

Raman spectroscopic measurements efficiently record the change in the local structure of the samples. Figure 3 shows the Raman peaks for the powder $Li_2Mn_{1-x}Ru_xO_3$ [x = 0.0, 0.1] samples sintered at 950 and 1050°C. Theoretical calculations predict the presence of 15 Raman active modes, including eight B_g modes and seven A_g modes [15].

The observed Raman peaks positions are summarized in Table 2 for the $Li_2Mn_{1-x}Ru_xO_3$ [x = 0.0, 0.1] compositions. The Raman spectra of the 950 and 1050°C sintered Li_2MnO_3 samples do not show significant changes in the peak positions. The Raman spectra of 950 and 1050°C sintered Ru doped $Li_2Mn_{0.9}Ru_{0.1}O_3$ show a change in the peak positions with Ru doping and changing sintering temperature. The results are shown in Table 2. The major A_g mode peak splits in two peaks for Ru doped $Li_2Mn_{0.9}Ru_{0.1}O_3$ for both the 950 and 1050°C sintered samples, while the initial composition shows only a single peak at ~615 cm^{-1}. The $Li_2Mn_{0.9}Ru_{0.1}O_3$ sample (950°C sintered) shows peaks at ~614 and ~603 cm^{-1}, while the 1050°C sintered sample shows peaks at ~620 and 607 cm^{-1}. Ru has a higher spin orbit coupling constant at 800 cm^{-1} and extended orbitals. It makes Ru-O bonds stronger than Mn-O, which is displayed in the shifting and splitting of the A_g peak. Other A_g and B_g peaks are also shifted in the Ru doped Raman spectra in comparison to the initial spectra.

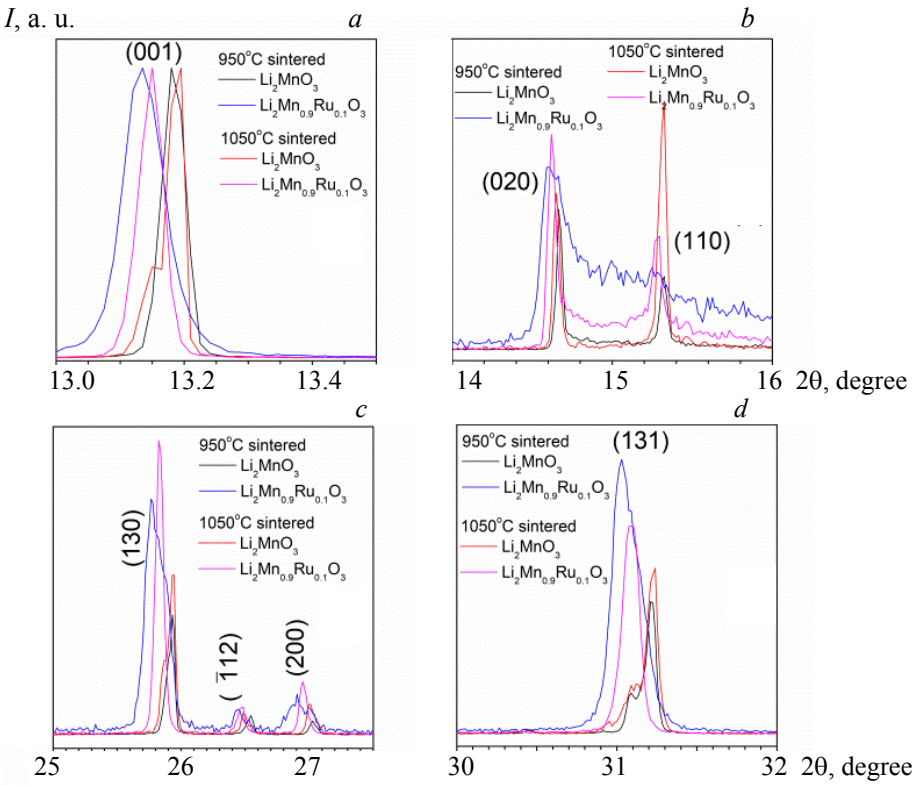

Fig. 2. Zoomed peaks of the synchrotron powder diffraction patterns of $Li_2Mn_{1-x}Ru_xO_3$ (x = 0.0 and 0.1) sintered at 950 and 1050°C.

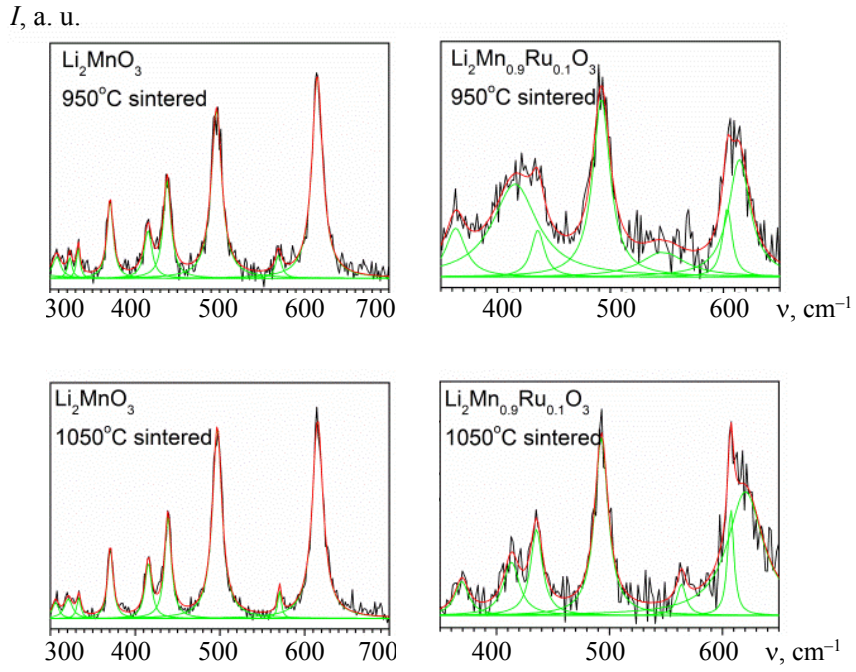

Fig. 3. Raman spectroscopy measurements of the $Li_2Mn_{1-x}Ru_xO_3$ (x = 0, 0.1) samples. The black line shows the experimentally observed spectra. The red line shows the whole fitting. The green lines show the position of peaks.

TABLE 2. Frequencies of the Experimentally Observed Raman Active Modes of $Li_2Mn_{1-x}Ru_xO_3$

Symmetry	Frequency theory, cm^{-1} [16, 17]	Frequency experiment, cm^{-1}			
		$x = 0$		$x = 0.1$	
		950°C	1050°C	950°C	1050°C
A_g	621	615	615	614	620
	577	569	570	603	607
	448	438	438	568	563
				435	435
B_{2g}	498	496	497	492	493
	496	415	415	415	413
	425	371	371	363	369
	377	333	333		

Figure 4 shows the impedance for the $Li_2Mn_{1-x}Ru_xO_3$ [$x = 0$, 0.1] samples sintered at 950 and 1050°C. All the compositions show a decrease in the impedance with the increase in frequency. $Li_2Mn_{0.9}Ru_{0.1}O_3$ sintered at 1050°C shows ~3×10^3 ohm impedance while the 950°C sintered composition shows ~3×10^4 ohm impedance. The Ru doping decreases the impedance of $Li_2Mn_{0.9}Ru_{0.1}O_3$ in comparison with the impedance of Li_2MnO_3. To reveal the reasons for the change in the structure, the splitting and shifting of the Raman peaks, and the change in impedance, we recorded synchrotron X-ray absorption data for all the samples.

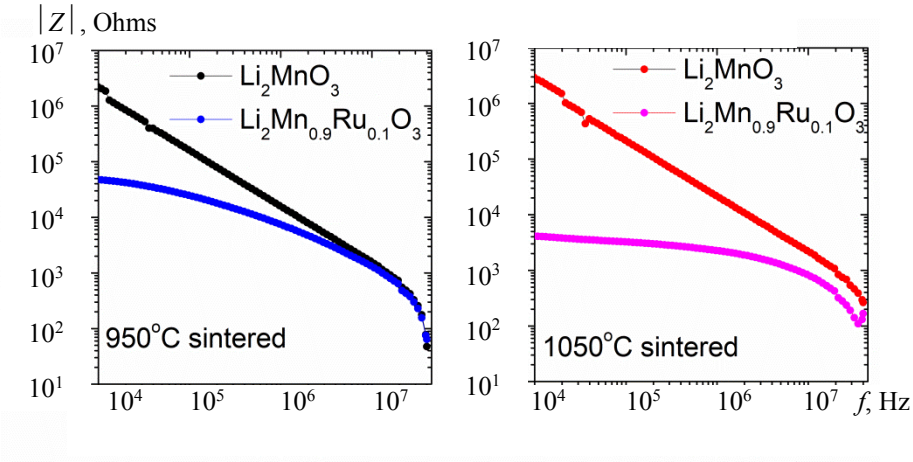

Fig. 4. Impedance versus frequency plots for $Li_2Mn_{1-x}Ru_xO_3$ [$x = 0.0$, 0.1] sintered at 950 and 1050°C.

Figure 5 shows the Ru-M_4 edge XAS spectra of the 950 and 1050°C sintered compositions of $Li_2Mn_{0.9}Ru_{0.1}O_3$. The XAS Spectra of RuO_2 and $LaMn_{0.8}Ru_{0.2}O_3$ were used as reference for the Ru^{+4} valence state, while the spectra of $Sr_4Ru_2O_9$ was used as reference for the Ru^{+5} valence state [18]. The M_4 edge peak was found at ~288 eV for RuO_2, which shows the presence of the Ru^{+4} valence state [12]. The M_4 edge peak was found at ~289.8 eV for $Sr_4Ru_2O_9$, which shows the presence of the Ru^{+5} valence state. Patra et al. showed the presence of the Ru^{+4} valence state in $LaMn_{0.8}Ru_{0.2}O_3$ [19]. We report the Ru-M_4 edge peak position at ~288 eV for $LaMn_{0.8}Ru_{0.2}O_3$, which indicates the presence of the Ru^{+4} valence state. Similarly, the M_4 edge peak was found at ~288.4 eV for the 1050°C sintered $Li_2Mn_{0.9}Ru_{0.1}O_3$, which shows the presence of the Ru^{+4} valence state. The M_4 edge containing the XAS peak was found at ~288.4 and 290 eV for the 950°C sintered $Li_2Mn_{0.9}Ru_{0.1}O_3$, which shows the presence of mixed valence states of Ru^{+4} and Ru^{+5}. Fitting of the M_4 edge spectra showed the quantity of Ru^{+4} 32% and Ru^{+5} 68% in the 950°C sintered $Li_2Mn_{0.9}Ru_{0.1}O_3$ [14]. Figure 6 shows the Mn-L_2 and L_3 edge absorption peaks for Mn_2O_3, MnO_2, $LiMn_2O_4$, Li_2MnO_3, and $Li_2Mn_{0.9}Ru_{0.1}O_3$. The Mn valence state was found to be Mn^{+3} in Mn_2O_3, Mn^{+4} in MnO_2, and 50–50% Mn^{+3}/Mn^{+4} in the $LiMn_2O_4$ reference compounds [11].

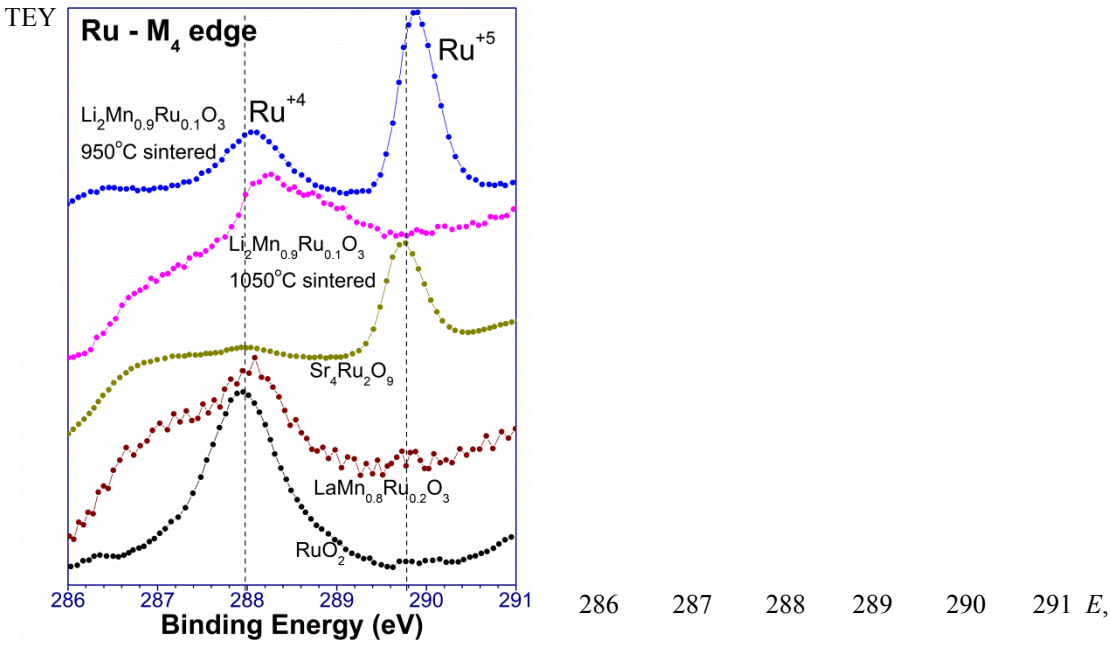

Fig. 5. X-ray absorption edge spectra for $Li_2Mn_{0.9}Ru_{0.1}O_3$. RuO_2, $LaMn_{0.8}Ru_{0.2}O_3$ and $Sr_4Ru_2O_9$ are used as reference samples for the Ru^{+4} and Ru^{+5} valence states.

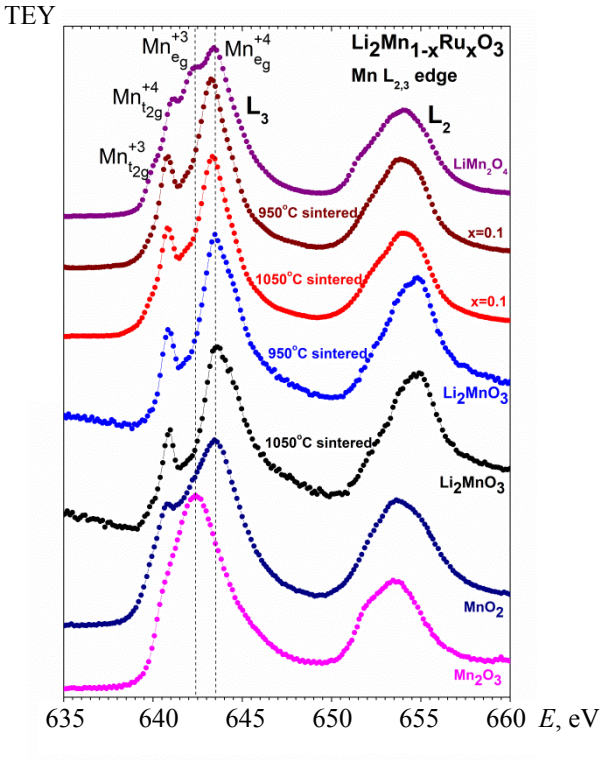

Fig. 6. X-ray absorption edge spectra showing the Mn-$L_{2,3}$ edge for Ru doped Li_2MnO_3 and the reference compounds.

We compared the Mn-L_2 and L_3 edge peaks of the 950 and 1050°C sintered Li_2MnO_3 and $Li_2Mn_{0.9}Ru_{0.1}O_3$ compositions with the L_2 and L_3 edge peaks of Mn_2O_3, MnO_2, and $LiMn_2O_4$. It was found that the L_3 peaks originated from the transition from $2p_{3/2}$ to $3de_g$ shifted in the 950°C sintered $Li_2Mn_{0.9}Ru_{0.1}O_3$ composition. These observations show the presence of the Mn^{+3}/Mn^{+4} valence state in the

950°C sintered $Li_2Mn_{0.9}Ru_{0.1}O_3$ composition, while the 1050°C sintered $Li_2Mn_{0.9}Ru_{0.1}O_3$ composition contains only the Mn^{+4} valence state. Figure 7 shows the O-K edge absorption peaks for the 950 and 1050°C sintered Li_2MnO_3 and $Li_2Mn_{0.9}Ru_{0.1}O_3$ compositions. Four major peaks *A*, *B*, *C*, and *D* are related to the transitions from O 1*s* to the hybridized states of the Mn 3*d*–O2*p* and Mn 4*sp*-O 2*p* orbitals. All the samples show *A*, *B* peaks, which correspond to the transition from O 1*s* to the hybridized states of the Mn^{+4} 3*d*–O2*p* orbitals, while *D* corresponds to the transition from O 1s to the hybridized states of the Mn 4*sp*-O 2*p* orbitals. Only the 950°C sintered $Li_2Mn_{0.9}Ru_{0.1}O_3$ composition shows the *C* peak, which is similar to the peaks observed in $LaMnO_3$ and corresponds to the transition between the Mn^{+3}3*d*–O2*p* orbitals (inset). It shows that the 950°C sintered $Li_2Mn_{0.9}Ru_{0.1}O_3$ composition has Mn^{+3} and Mn^{+4} mixed valences, while the 1050°C sintered $Li_2Mn_{0.9}Ru_{0.1}O_3$ composition has only the Mn^{+4} valence state.

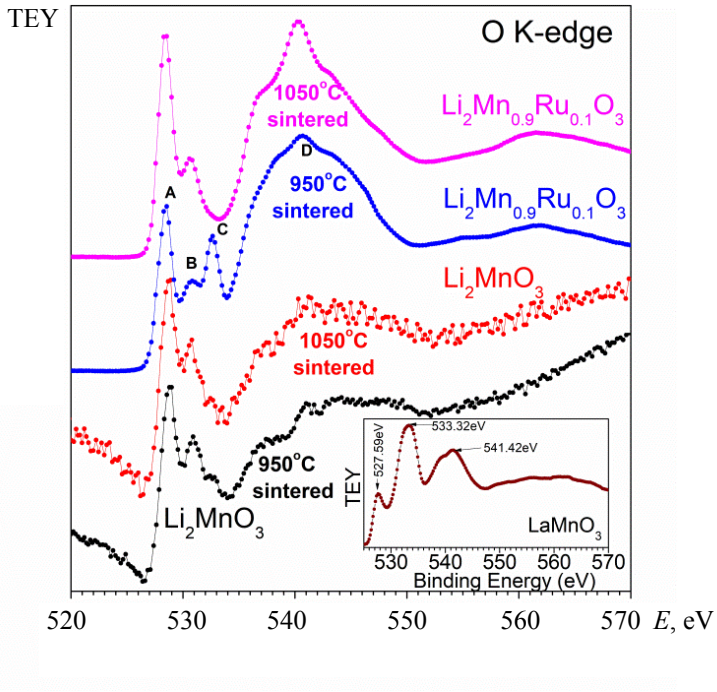

Fig. 7. X-ray absorption edge spectra showing the O-K edge for the parent and Ru doped Li_2MnO_3.

The synchrotron X-ray diffraction study shows the change in the lattice parameters and volume of the unit cell of Li_2MnO_3 with Ru doping at the Mn site. The lattice parameters and volume of the unit cell further change with varying sintering conditions for the Ru-doped composition. The Raman spectra of the Ru-doped composition shows the sifting and splitting in vibrational peaks. X-ray absorption spectroscopic measurements show the presence of Mn^{+3}, Mn^{+4}, Ru^{+4}, and Ru^{+5} mixed valence states in the 950°C sintered $Li_2Mn_{0.9}Ru_{0.1}O_3$ composition. The ionic size of these valence states was found to be 0.645 Å for Mn^{+3}, 0.53 Å for Mn^{+4}, 0.62 Å for Ru^{+4}, and 0.565 Å for Ru^{+5} [5, 9]. The presence of Ru^{+5} along with Mn^{+3} increases the size of the unit cell of 950°C sintered $Li_2Mn_{0.9}Ru_{0.1}O_3$. In should be noted that the increase in the size of the unit cell for 1050°C sintered $Li_2Mn_{0.9}Ru_{0.1}O_3$ remains smaller than for 950°C sintered $Li_2Mn_{0.9}Ru_{0.1}O_3$. However, these Ru-doped compositions show an increased size of the unit cell in comparison with the 950 and 1050°C sintered initial Li_2MnO_3. These findings show that Ru substitution at the Mn site produces Mn^{+4} and Ru^{+4} in 1050°C sintered $Li_2Mn_{0.9}Ru_{0.1}O_3$, while Mn^{+3}, Mn^{+4}, Ru^{+4}, and Ru^{+5} mixed valence states exist in the 950°C sintered $Li_2Mn_{0.9}Ru_{0.1}O_3$ composition. Shifting and splitting in the Raman spectra were found due to the presence of the Ru-O bond and Mn^{+3}-O bonds. The Mn^{+3} has the biggest size among the Mn^{+3}, Mn^{+4}, Ru^{+4}, and Ru^{+5} valence states. The presence of the Mn^{+3} valence state leads to Jahn-Teller distortion due to the presence of one e_g electron in it [9]. The specific sintering conditions change the valence states of Mn and Ru in Ru doped Li_2MnO_3. By utilizing these mixed valences, samples can be prepared for the required cathode material and catalytic applications.

Conclusions. We have documented the experimental evidence of the sintering temperature dependent Ru mixed valences of Ru^{+4} and Ru^{+5} using M_4 absorption edge in the X-ray absorption spectra. Peaks of the O-K edge for 950ºC sintered $Li_2Mn_{0.9}Ru_{0.1}O_3$ show the presence of Mn^{+3}-O and Mn^{+4}-O hybridization. The 1050ºC sintered Li_2MnO_3 and $Li_2Mn_{0.9}Ru_{0.1}O_3$ samples show evidence of Mn^{+4} and Ru^{+4} valences. The Raman spectra show shifting and splitting with Ru doping at the Mn site in Li_2MnO_3. Synchrotron X-ray diffraction patterns show the highest change in the size of the unit cell of 950ºC sintered $Li_2Mn_{0.9}Ru_{0.1}O_3$ in comparison with other compositions.

Acknowledgments. B. Singh thanks the UGC-DAE-CSR, Indore Centre for providing financial support under the CRS project scheme and Priyanka for the project fellowship. BS also thanks prof ACP for Raman measurements and DST (India) for providing instrumental support to the Centre of Material Sciences from its FIST funding scheme.

REFERENCES

1. R. Marom, S. F. Amalraj, N. Leifer, D. Jacob, D. Aurbach, *J. Mater. Chem.*, **21**, 9938–9954 (2011).
2. B. L. Ellis, K. T. Lee, L. F. Nazar, *Chem. Mater*., **22**, 691–714 (2010).
3. K. S. Kang, Y. S. Meng, J. Breger, C. P. Grey, G. Ceder, *Science*, **311**, 977–980 (2006).
4. M. Sathiya, K. Ramesha, G. Rousse, D. Foix, D. Gonbeau, A. S. Prakash, M. L. Doublet, K. Hemalatha, J. M. Tarascon, *Chem. Mater*., **25**, 1121–1131 (2013).
5. S. S. Manoharan, R. K. Sahu, *Chem. Commun.* (Cambridge), 3068–3069 (**2002**), doi: 10.1039/B209293
6. Y. Lyu, E. Hu, D. Xiao, Y. Wang, X. Yu, G. Xu, S. N. Ehrlich, K. Amine, L. Gu, X. Yang, H. Li, *Chem. Mater*., **29**, 9053–9065 (2017).
7. M. Sathiya, J.-B. Leriche, E. Salager, D. Gourier, J.-M. Tarascon, H. Vezin, *Nat. Commun.*, **6**, 6276 (2015).
8. D. Mori, H. Kobayashi, T. Okumura, H. Nitani, M. Ogawa, Y. Inaguma, *Solid State Ion.*, **285**, 66–74 (2016).
9. B. Singh, S. S. Manoharan, M. L. Rao, S. P. Pai, *Phys. Chem. Chem. Phys.*, **6**, 4199–4202 (2004).
10. B. Singh, *Phys. Chem. Chem. Phys.*, **18**, 12947–12951 (2016).
11. M. V. Reddy, S. S. Manoharan, J. John, B. Singh, G. V. S. Rao, B. V. R. Chowdari, *J. Electrochem. Soc.*, **156**, A652–A660 (2009).
12. J. G. Zhou, H. T. Fang, Y. F. Hu, T. K. Sham, C. X. Wu, M. Liu, F. Li, *J. Phys. Chem. C*, **113**, 10747–10750 (2009).
13. T. Harano, G. Shibata, K. Ishigami, Y. Takashashi, V. K. Verma, *Appl. Phys. Lett.*, **102**, 222404 (1–4) (2013).
14. B. Singh, P. Singh, *SN Appl. Sci*., **2**, 506 (2020).
15. R. E. Ruther, H. Dixit, A. M. Pezeshki, R. L. Sacci, V. R. Cooper, J. Nanda, G. M. Veith, *J. Phys. Chem. C*, **119**, 18022–18029 (2015).
16. C. M. Julien, M. Massot, *Mater. Sci. Eng. B*, **100**, 69–78 (2003).
17. S. F. Amalraj, D. Sharon, M. Talianker, C. M. Julien, L. Burkala, R. Lavi, E. Zhecheva, B. Markovsky, E. Zinigrad, D. Kovacheva, *Electrochim. Acta*, **97**, 259–270 (2013).
18. Z. Hu, H. V. Lips, M. S. Golden, J. Fink, G. Kaindl, F. M. F. deGroot, S. Ebbinghaus, A. Reller, *Phys. Rev. B*, **61**, 5262–5266 (2000).
19. A. S. Patra, G. Gogoi, R. K. Sahu, M. Qureshi, *Phys. Chem. Chem. Phys.*, **19**, 12167–12174 (2017).